IOP Publishing and International Atomic Energy Agency Nuclear Fusion
Nucl. Fusion **47** (2007) 378–386 doi:10.1088/0029-5515/47/5/002

Joint experiments on small tokamaks: edge plasma studies on CASTOR

G. Van Oost[1], M. Berta[2,13], J. Brotankova[3], R. Dejarnac[3], E. Del Bosco[4], E. Dufkova[3], I. Ďuran[3], M.P. Gryaznevich[5], J. Horacek[3], M. Hron[3], A. Malaquias[6], G. Mank[6], P. Peleman[1], J. Sentkerestiova[3], J. Stöckel[3], V. Weinzettl[3], S. Zoletnik[2], B. Tál[2], J. Ferrera[4], A. Fonseca[7], H. Hegazy[8], Y. Kuznetsov[7], A. Ossyannikov[9], A. Singh[10], M. Sokholov[11] and A. Talebitaher[12]

[1] Department of Applied Physics, Ghent University, Ghent, Belgium
[2] KFKI-RMKI, Association EURATOM, Budapest, Hungary
[3] Institute of Plasma Physics, Association EURATOM/IPP.CR, Prague, Czech Republic
[4] INPE, São José dos Campos, Brazil
[5] EURATOM/UKAEA Fusion Association, Culham Science Centre, Abingdon, UK
[6] IAEA, NAPC Physics Section, Vienna, Austria
[7] Institute of Physics, University of São Paulo, Brazil
[8] EAEA, Cairo, Egypt
[9] Saint Petersburg State University, Russia
[10] Plasma Physics Laboratory, University of Saskatchewan, Canada
[11] RRC 'Kurchatov Institute', Moscow, Russia
[12] Plasma Physics Research Center, Teheran, Iran
[13] Széchenyi István University, Association EURATOM, Gyõr, Hungary

Received 21 December 2006, accepted for publication 4 April 2007
Published 25 April 2007
Online at stacks.iop.org/NF/47/378

Abstract
The 1st Joint (Host Laboratory) Experiment on 'joint research using small tokamaks' was carried out using the IPP Prague experimental facility 'CASTOR tokamak'. The main experimental programme was aimed at characterizing the edge plasma in a tokamak by using different advanced diagnostic techniques. It is widely recognized that characterization of phenomena occurring at the plasma edge is essential for understanding the plasma confinement in a tokamak. The edge plasma in small and large scale experiments has many similar features, and the results obtained through detailed measurements in a small flexible device such as CASTOR are in many aspects still relevant to those in large tokamaks. Therefore, it is expected that the results of this joint experiment will have general validity. The radial and poloidal structure of electrostatic turbulence was characterized. The effects of edge biasing were analysed. Radiation fluctuations and profile measurements were performed using fast bolometry. Plasma position measurements were performed using novel Hall sensors.

PACS numbers: 52.55.Fa

(Some figures in this article are in colour only in the electronic version)

1. Introduction

The first Joint (Host Laboratory) Experiment (JE) on 'joint research using small tokamaks' (JRUST) involving twenty scientists from seven countries was carried out between 28 August and 9 September 2005 on the CASTOR tokamak at the Institute of Plasma Physics of the Academy of Sciences of the Czech Republic (IPP-ASCR), and was jointly organized by IPP-ASCR and KFKI (Central Research Institute for Physics of the Hungarian Academy of Sciences) Budapest. It was coordinated by the International Atomic Energy Agency (IAEA) in the framework of the Coordinated Research Project (CRP) JRUST and supported through IAEA and International Centre for Theoretical Physics (ICTP). The objective of the joint experiment was to perform studies on the topics of plasma edge turbulence and plasma confinement based on broad international participation to benefit from the added value of the exchange of international expertise. Edge plasma studies have a long tradition on the CASTOR tokamak (appropriate equipment, recognized expertise, etc) (see e.g. 1–3). Another

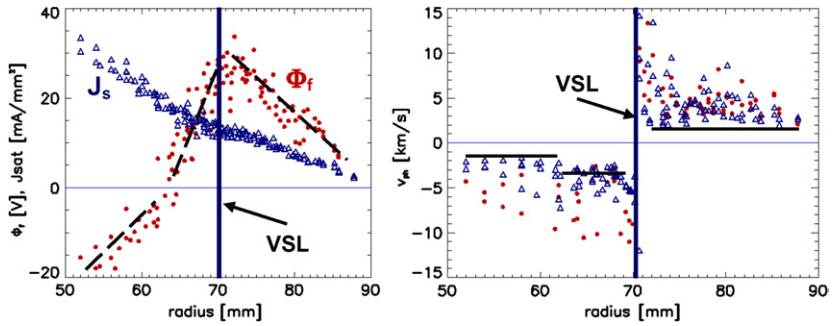

Figure 1. Left graph: radial profiles of floating potential Φ_f (red circles) and density of ion saturation current J_{sat} ($J_{sat} = I_{sat}/A$, A is $2\pi \times$ radius $\times$ length of the probe). Right graph: phase velocities of fluctuations obtained from Φ_f (red circles), and J_{sat} (blue triangles). Horizontal lines in the right panel show velocities calculated from the gradient of Φ_{fl}. Both radial profiles are measured at the top of the torus.

goal of this joint experiment was the development of tools for remote participation and data exchange. These two aims are expected to follow and contribute to some extent to a pool of knowledge in support of the ITER project, as the JE was performed under an intensive international cooperation and with an important component of remote operation and data exchange. The role and contribution of small tokamaks to the topics of expertise exchange and remote operation is highlighted by this initiative.

The experimental set-up is briefly described in section 2. In section 3 the main experimental results are given: radial and poloidal electrostatic edge turbulence structure, magnetic measurements using Hall sensors, effects of electrode edge biasing, radiation fluctuations and profile measurements using fast bolometry and development of standard interfaces for remote participation and data exchange. A discussion and some conclusions are presented in section 4.

2. Experimental set-up

The particular feature of the experiment is the exploitation of unique diagnostics to study the physics of the edge plasma in detail. During the experiments, electric fields were generated by biasing an electrode inserted into the edge plasma to modify the turbulence and transport behaviour in this region. The CASTOR tokamak ($R = 0.4$ m, $a = 85$ mm, $B_t < 1.5$ T, $I_p < 25$ kA, $\tau_{pulse} < 50$ ms, $0.5 < n_e(10^{19}\,\mathrm{m}^{-3}) < 3.0$, $T_e(0) < 200$ eV) is equipped with a circular cross section poloidal limiter, and with a standard set of diagnostic tools. During these joint experiments the available diagnostic systems were two bolometric arrays for the fast measurement of radiation losses, Langmuir probe arrays for edge plasma monitoring in radial and poloidal directions, directional (Gundestrup) probes for parallel and perpendicular plasma flow determination and a full poloidal array of magnetic pick-up coils and Hall sensors for plasma position monitoring. The H_α diagnostic was located at the top of the vessel at the same toroidal location of the rake probes to monitor the radiation due to recycling with a sampling frequency of 40 kHz. The data acquisition system consists of 24 channels (40 kHz) to measure the basic plasma parameters and 96 channels (1 MHz) for the fast measurement of the edge plasma parameters. The software developed for data acquisition control and for data processing is based on widely used IDL® and/or MATLAB® environment.

3. Experiments and results

3.1. Radial edge turbulence structure

The edge plasma and the electrostatic turbulence were characterized using a radial array consisting of a double rake probe with 16 Langmuir tips each (the radial separation between two adjacent pins is 2.5 mm) inserted into the edge plasma from the top of the torus. The time evolution of the radial profiles of electron temperature and density was measured during a single shot. Furthermore, from the time shift between the signals of two poloidally separated tips it was possible to determine the poloidal velocity of fluctuating density and plasma floating potential structures. Since these time shifts were typically lower than the sampling rate (1 μs), two statistical techniques were developed allowing the determination of the correlation length and phase velocity of potential fluctuations during a single shot: (i) polynomial curve fitting (fitting the cross-correlation by some polynomial function) and (ii) linear fitting of the phase function of the cross-power spectral density. Both techniques provided similar results, as illustrated in figure 1. Both methods diverge in the proximity of the last closed flux surface (LCFS), which is associated with the maximum of the floating potential seen in the left graph of figure 1. However, the position of the velocity shear layer (VSL) can be identified with a precision of ~1 mm, as seen in figure 1. From the gradient of the floating potential (dashed line in the left graph of figure 1), the phase velocities were roughly estimated as $v_{ph} = E_r/B$, where E_r is estimated as grad Φ_f, neglecting the gradient of the electron temperature. In the right graph of figure 1, the velocities are depicted as three horizontal lines (in the region $50 < r < 60$ mm $v_{ph} = -1.4\,\mathrm{km\,s^{-1}}$, for $60 < r < 70$ mm $v_{ph} = -3.3\,\mathrm{km\,s^{-1}}$, and for $70 < r < 90$ mm $v_{ph} = 1.3\,\mathrm{km\,s^{-1}}$). It is evident that experimental points are above these lines, which implies that the electron temperature gradient cannot be fully neglected, if a precise comparison of the phase and $E \times B$ velocity is required. In spite of a large shear, the levels of density and potential fluctuations do not change in the proximity of the velocity shear layer. Finally, it is interesting to note that the phase velocity of density fluctuations is systematically lower than that of potential fluctuations. The explanation of this observation requires more analysis.

Furthermore, from the spatio-temporal behaviour of cross-correlation functions of radially separated tips, a radial size

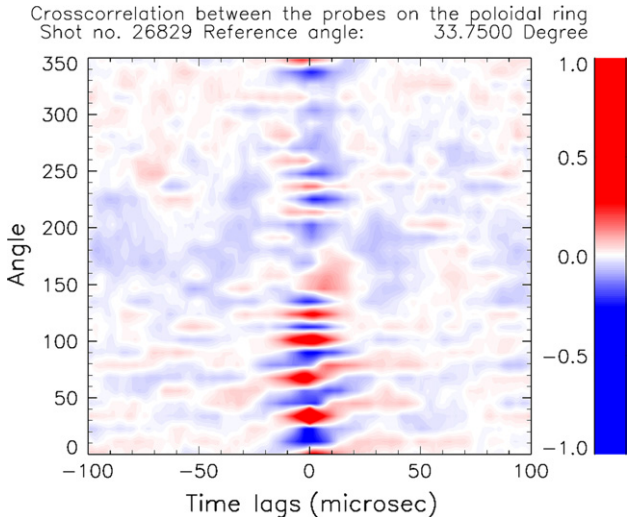

Figure 2. A spatio-temporal correlation function along the poloidal ring of probes. The reference probe is at 33.75° relative to the equatorial plane at the LCFS.

of the fluctuating structures of about 10 mm was determined during this experimental campaign.

It may also be noted that the radius of the LCFS (and also the VSL) at the top of the torus is noticeably smaller than that of the limiter radius. This is because of a downward shift of the plasma column on CASTOR [1, 2].

3.2. Poloidal edge turbulence structure

The phase velocity of potential fluctuations in the poloidal direction was measured in discharges with and without biasing using a poloidal array of 96 Langmuir probes arranged uniformly poloidally at one toroidal position. Due to a limited number of digitizers only 32 channels could be measured simultaneously. In most measurements every third probe was used, but occasionally the local structure was studied by digitizing all signals from a limited poloidal range. Data measured by the poloidal ring was evaluated by correlation techniques. A typical correlation plot is shown in figure 2, where the x-axis is the time lag and the y-axis is the poloidal angle.

Spatial wave-like structures (electromagnetic features of turbulence) were observed in the correlation figures between 355° and 135° (0 is at the low field side). In other regions (e.g. at the top) the wave-like structure was not obvious but a localized correlation extending over a couple of probes was seen. The difference in behaviour at different locations is believed to be due to misalignment of the probe array relative to the LCFS.

In order to determine the temporal change of the amplitude of the wave-like structure the spatial correlation functions were used as filter functions: at each time the detrended signals were multiplied by the cross-correlation value at 0 time lag and all 32 values were summed up. The resulting time signal contains dominantly the amplitude of the wave-like structure, the local fluctuations being suppressed by summation. This filtered signal was squared and normalized by its scatter (σ) in order to show the temporal change in the relative amplitude of the power of the wave-like structure (figure 3.).

The filtered signal is obviously highly intermittent and pronounced peaks (greater than 3σ) can often be seen, in contrast to the signals of the individual Langmuir probes which are very close to Gaussian. This demonstrates that the temporal behaviour of the wave-like poloidally extended structures and the local turbulence is very different, and over the whole array the signal of a given Langmuir probe is composed of a mixture of these two components: one with a short poloidal correlation (cm scale) and another one with wave-like character correlated with a large poloidal extent. The mode number of this wave-like phenomenon approximately matches the edge safety factor value. A long toroidal correlation length (correlation value above 0.8 over one half of the toroidal circumference) between certain rake probe and ring probe pins could be observed, when these pins were located on the same flux tube.

3.3. Magnetic measurements using an array of low-cost commercial Hall sensors

As the discharges became longer in large tokamaks, the evaluation of B from its measured time derivative has become increasingly difficult, because the integration needs a precise determination of possible offsets in the preamplifiers. In the past, standard Hall probes have been used to measure the absolute value of B directly together with its fluctuations in the boundary plasma of tokamaks [4].

Advancements in semiconductor technology hand in hand with a broad spectrum of industrial applications have driven the development of new types of Hall sensors for magnetic measurements in recent years. A particular advancement is the availability of 'integrated' Hall transducers, where the sensing element together with the complex electronic circuitry is integrated on a single small chip with characteristic dimension of a few millimetres. The on-chip integrated circuits provide stabilization of the supply voltage, output voltage amplification, signal conditioning in order to suppress the high frequency noise and elimination of temperature dependence of the sensor's output. In particular, the output amplifier placed directly beside the sensing element significantly improves the frequency response and the signal to noise ratio. Because of the widespread industrial use of such sensors, their cost is rather low (of the order of 1 Euro/piece). We report in this paper about the first tests of this new type of Hall sensors in a tokamak in-vessel environment (CASTOR). The 16 Hall sensors of the A1322LUA type produced by Allegro MicroSystems, Inc. were mounted on a stainless steel ring symmetrically encircling the CASTOR plasma in the poloidal direction 10 mm outside the limiter radius. The Hall sensors were oriented such that they measured the poloidal magnetic field. Special adjustable holders were used in order to ensure proper alignment and consequently to minimize the cross-talk from the about 50 times stronger toroidal magnetic field. A traditional magnetic pick-up coil was fixed near each Hall sensor for reference and also for envisaged MHD studies. The sensors have a nominal sensitivity of 31.25 mV mT^{-1} and dynamic range ±80 mT. The peak-to-peak noise level is below 1 mT. The bandwidth specified by the manufacturer is 30 kHz. The operating temperature range is from −40 to 150 °C. A supply voltage of 5 V is needed to drive each Hall sensor. The sensor calibration in the frequency range 1–20 kHz is plotted in figure 4.

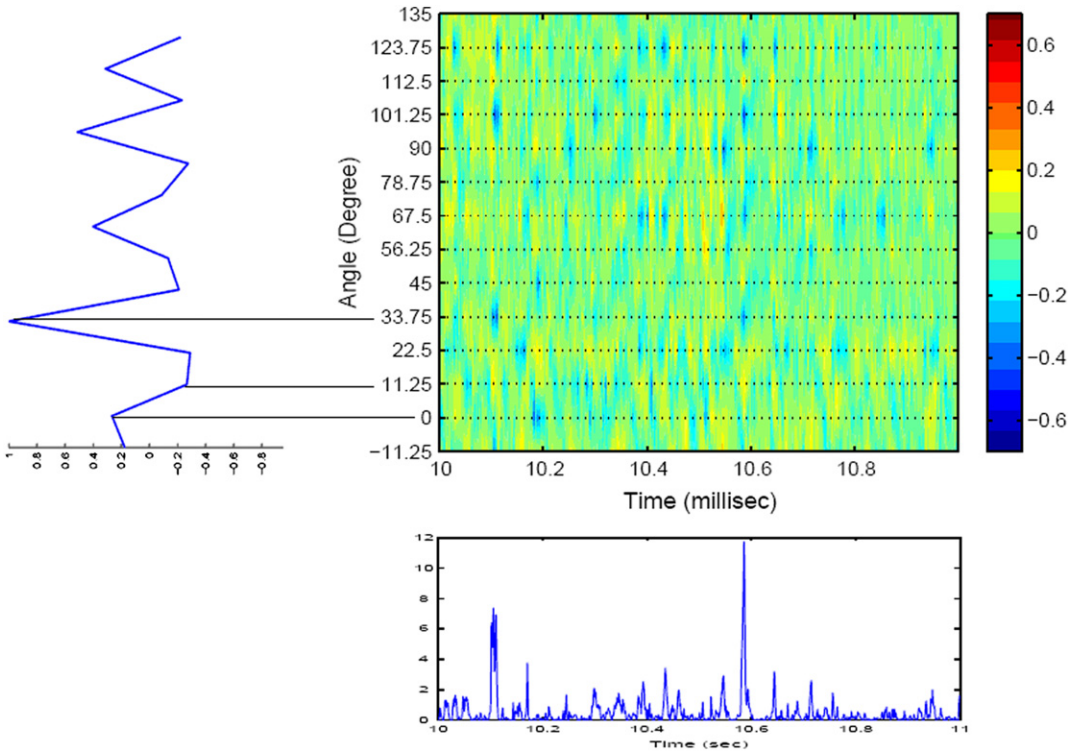

Figure 3. Illustration of the filtering method. The top colour plot shows the time evolution of the signals where the wave-like structure is visible. After filtering we get the signal shown at the bottom.

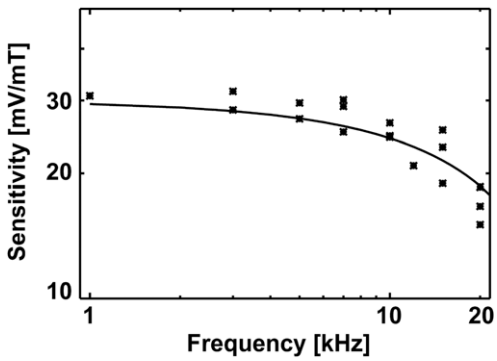

Figure 4. Calibration curve of the A1322LUA Hall sensor in the frequency band 0–20 kHz

The frequency response of the sensors was found to be reasonably flat up to 10 kHz, which is sufficient, e.g. for plasma position measurements on CASTOR. Additionally, dc calibration of each Hall sensor was performed using standard Helmholtz coils. The importance of the planar Hall voltage generated by a strong toroidal magnetic field (∼1.2 T on CASTOR) oriented parallel to the sensor's plane was investigated. For this purpose several vacuum field pulses were made, charging only the poloidal field coils and creating a known calibrating magnetic field. In addition, the toroidal field coils were energized, creating a toroidal magnetic field perpendicular to the calibration magnetic field. The difference in sensor's output with and without the toroidal magnetic field was well below its noise level. Thus, the contribution of the planar Hall effect to the sensor's output voltage was found to be negligible. On CASTOR the sensors were operated at rather stable temperature close to room temperature. Nevertheless, the possible temperature dependence of the sensor's output was checked keeping in mind the possible use of these sensors in middle sized fusion devices, where temperature variations over a single pulse can become significant. Temperature changes were obtained by routine inductive heating of the CASTOR vacuum vessel performed at the beginning of each experimental day. Again, the changes of the sensor's output voltage (with only the poloidal field coils energized) due to thermal loading were found well below the noise level for temperatures 20–100 °C.

The comparison of the poloidal magnetic field B_θ evaluated from the Hall sensors located at the low field side (LFS) and the high field side (HFS) mid-plane and from nearby pick-up coils during a standard CASTOR discharge with plasma current of 10 kA and line-averaged plasma density of $9 \times 10^{18}\,\mathrm{m}^{-3}$ is plotted in figure 5. The evolution of plasma current during this CASTOR discharge is shown for comparison.

Thanks to the knowledge of the absolute value of the magnetic field provided by the Hall sensors, we were able to correct the linear drift of the numerically integrated coils data. The drift is caused by the finite resolution of A/D converters. There is perfect agreement between the output of the Hall sensors and the corrected and numerically integrated signals of the pick-up coils. There is an apparent 'anti-phase' evolution of the magnetic signals measured at LFS and HFS during the flat-top phase of the discharge. This observation together with the evolution of the plasma current monotonously decreasing from 10.5 to 8.7 kA is interpreted as a movement of the plasma current channel. In the initial phase of the discharge the plasma is moving towards the LFS and after 17 ms it drifts

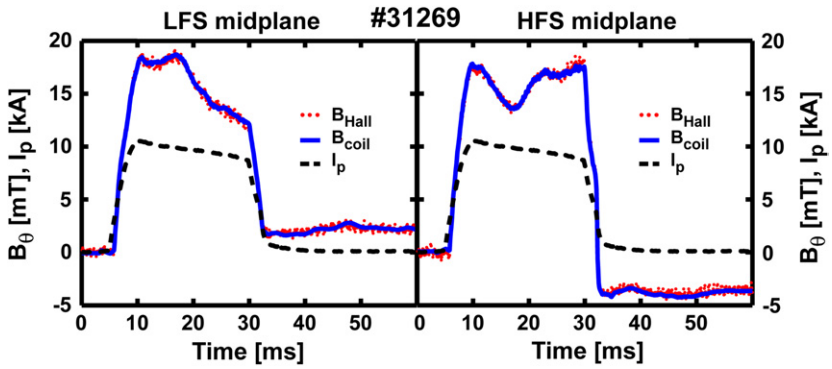

Figure 5. Poloidal magnetic field measured by the Hall sensors (red dots) and the neighbouring pick-up coils (blue) at the LFS mid-plane (left panel) and the HFS mid-plane (right-panel) during the CASTOR discharge #31269. Temporal evolution of the plasma current (dashed line) is plotted in both panels for comparison. Notice the remaining magnetic field of a few milliteslas caused by a current in the tokamak primary windings which persists long after the termination of the plasma discharge.

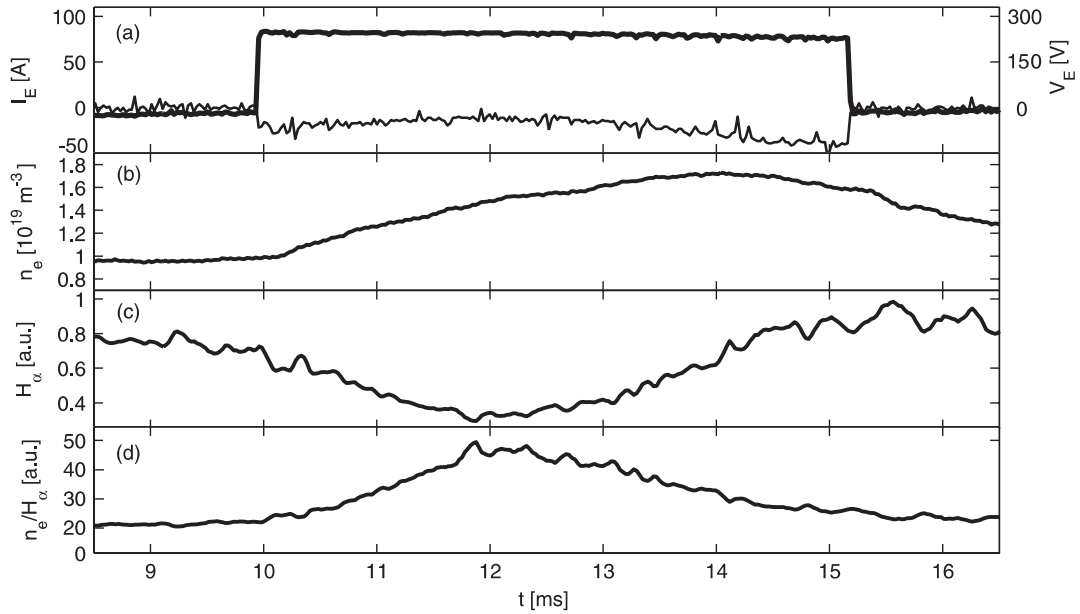

Figure 6. Time evolution of plasma parameters of a typical edge electrode biasing experiment on CASTOR. (*a*) the electrode voltage V_{E} (thick line) and current I_{E} (thin line), (*b*) the central line-averaged electron density $\bar{n}_{\mathrm{e}}$, (*c*) H_α radiation and (*d*) the ratio of $\bar{n}_{\mathrm{e}}/H_\alpha$.

back towards the HFS. Note that a significant magnetic field of a few milliteslas remains long after the termination of the plasma discharge. This remaining magnetic field was found to be induced by a current flowing in the primary winding of the tokamak and remains significant for about 300 ms after the termination of the plasma. As a result, it is not possible to remove drifts associated with integrated pick-up coils signals supposing the zero-field state immediately after the termination of CASTOR discharge, which was a common practice before.

In conclusion, the A1322LUA type integrated Hall sensors produced by Allegro MicroSystems, Inc. were tested for the first time in a tokamak environment on CASTOR, and they were found to qualify for in-vessel use of small to middle sized fusion devices where radiation is not an issue. They offer an attractive alternative to traditional pick-up coils for applications where a good frequency response up to 10 kHz is sufficient and the temperature below 150 °C can be guaranteed. The main advantages over the traditional pick-up coils are the smaller size and more straightforward interpretation of the output without the need of rather cumbersome integration and drift removal procedure associated with the use of inductive loops. Further exploitation of these sensors is envisaged particularly to improve the precision of the plasma position measurement.

3.4. Edge biasing

Positive electrode edge biasing experiments were performed to demonstrate the effects of electric fields on the main plasma parameters. Figure 6 shows time traces of electrode voltage (V_{E}) and current (I_{E}), central line-averaged density $\bar{n}_{\mathrm{e}}$, H_α emission and ratio of $\bar{n}_{\mathrm{e}}/H_\alpha$. Before biasing, the electrode (inserted from the top and positioned at radius $r_{\mathrm{E}} = 40$ mm) was floating such that no current flowed between the electrode

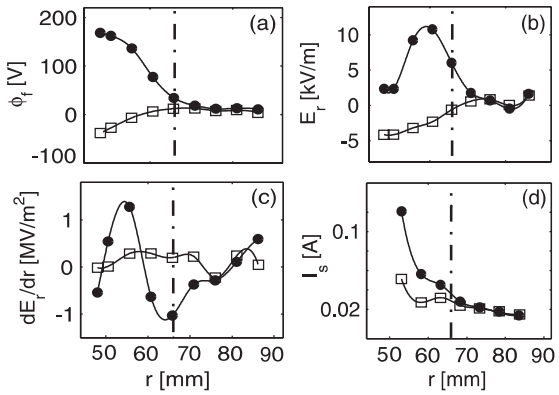

Figure 7. Radial profiles of (a) the floating potential ϕ_f, (b) the radial electric field E_r, (c) E_r the shear and (d) the ion saturation current I_s averaged over 4 ms before (open symbols) and during (filled symbols) biasing. The vertical dashed–dotted line marks the position of the LCFS.

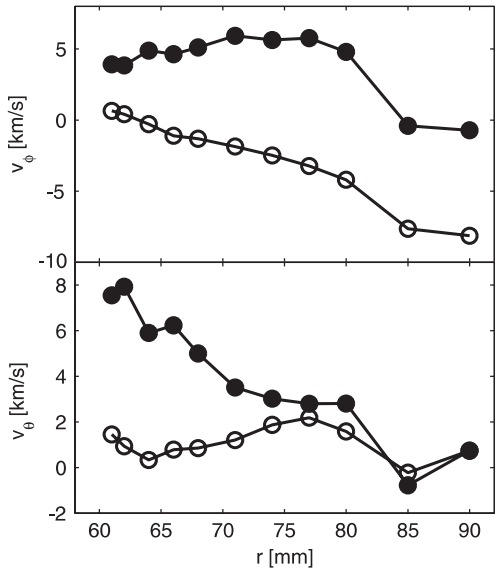

Figure 8. Radial profiles of the toroidal velocity v_ϕ and poloidal velocity v_θ averaged over 4 ms before (open circles) and during (filled circles) biasing.

and the vessel. At about 10 ms after the start of the plasma discharge, a positive biasing pulsed voltage $V_E \approx 260$ V is applied for a period of ∼5 ms, during which an average current of about $I_E = 20$ A is drawn by the electrode, as seen in figure 6(a). In figure 6(b), it can be seen that during biasing, $\bar{n}_e$ is built-up gradually and reaches a maximum at $t = 14$ ms before slowly falling off to its original pre-bias value. In the initial stage of the biasing, from 10 to 12.5 ms, there is a clear reduction in recycling indicated by a drop in H_α emission, and thus, a net increase of the ratio $\bar{n}_e/H_\alpha$ (which is roughly proportional to the particle confinement time τ_p) by a factor of 2.5 with respect to the pre-bias phase, as seen in figures 6(c) and (d), respectively. The plasma position remains stationary during the biasing phase. These results indicate an improvement of the global particle confinement induced by electrode positive biasing, as observed earlier [3].

Figure 7 further illustrates the influence of positive biasing on the radial profile of edge plasma parameters. The radial profiles of floating potential ϕ_f, radial electric field E_r and its shear dE_r/dr and ion saturation current I_s are obtained by averaging over a time window of 4 ms before (open symbols) and during (filled symbols) the biasing phase. Here, E_r is calculated directly from the radial derivative of ϕ_f measured at $r = 60$ mm on two adjacent pins neglecting the contribution from the T_e gradient, and therefore underestimating E_r slightly. These approximations are justified due to the very slight changes in edge T_e and ∇T_e before and during the biasing phase observed in similar biasing experiments. The radial position of the LCFS is around $r_{LCFS} = 66$ mm (indicated by the dashed–dotted line in the figures). During the biasing phase, the radial dependence of ϕ_f is strongly modified, as shown in figure 7(a), leading to a narrow positive and single-peaked E_r structure with a maximum of 11 kV m^{-1} at $r \approx 61$ mm, just inside the LCFS (see figure 7(b)). As a consequence, a strong positive (∼1.3 MV m^{-2}) and negative (∼-1MV m^{-2}) E_r shear are generated inside and across the LCFS, respectively, as shown in figure 7(c). The maximum shear rate of the $E_r \times B$ flow, $\tau_s^{-1} \propto dv_{\vec{E}\times\vec{B}}/dr$, is thus about (1–1.3) × 10^6 s^{-1}. On the other hand, the decorrelation rate of local turbulence scattering, τ_{c0}^{-1}, calculated from the e-folding time of the autocorrelation function of I_s fluctuation data detected before biasing, gives $\tau_{c0}^{-1} = 1.6 \times 10^5$ s^{-1}. Hence, the flow shear rate exceeds significantly the turbulence scattering rate, and thus turbulence and turbulent transport are suppressed. The reduction in I_s and ϕ_f fluctuations during biasing has been observed in the experiments. The reduced turbulent transport leads to the formation of an edge pedestal and thus to a steepening of the edge density profile during biasing, as shown in figure 7(d). It can be concluded that a clear and reproducible transition to improved confinement is induced by the edge electrode biasing along with the creation of a particle edge transport barrier just inside the LCFS. This barrier is characterised by (i) a substantial increase of the edge density gradient; (ii) a reduction in recycling indicated by a drop in H_α signal (as shown in figure 6); (iii) a substantial increase of the global particle confinement time (as shown in figure 6) and (iv) suppression of the density and potential fluctuation level.

Flow measurements were performed using a Gundestrup probe with eight collectors [5]. The time evolution of the radial profiles of floating potential, radial electric field, parallel and perpendicular Mach numbers was obtained in the biased and ohmic phases of a single discharge. The poloidal velocity v_θ and the toroidal velocity v_ϕ shown in figure 8 are deduced from these Gundestrup probe data using an improved one-dimensional fluid probe model in which a constant $T_e = 35$ eV is assumed. The radial flow profiles were measured in a shot-to-shot scan in reproducible discharges. It is found that not only the perpendicular but also the parallel flow increases during biasing.

Flow velocities measured by the Gundestrup probe and the phase velocity of fluctuations were compared on CASTOR already earlier [6]. The good correlation between these two quantities as well as with the $E \times B$ drift indicates that the turbulent structures are ‘frozen’ into the poloidally rotating plasma.

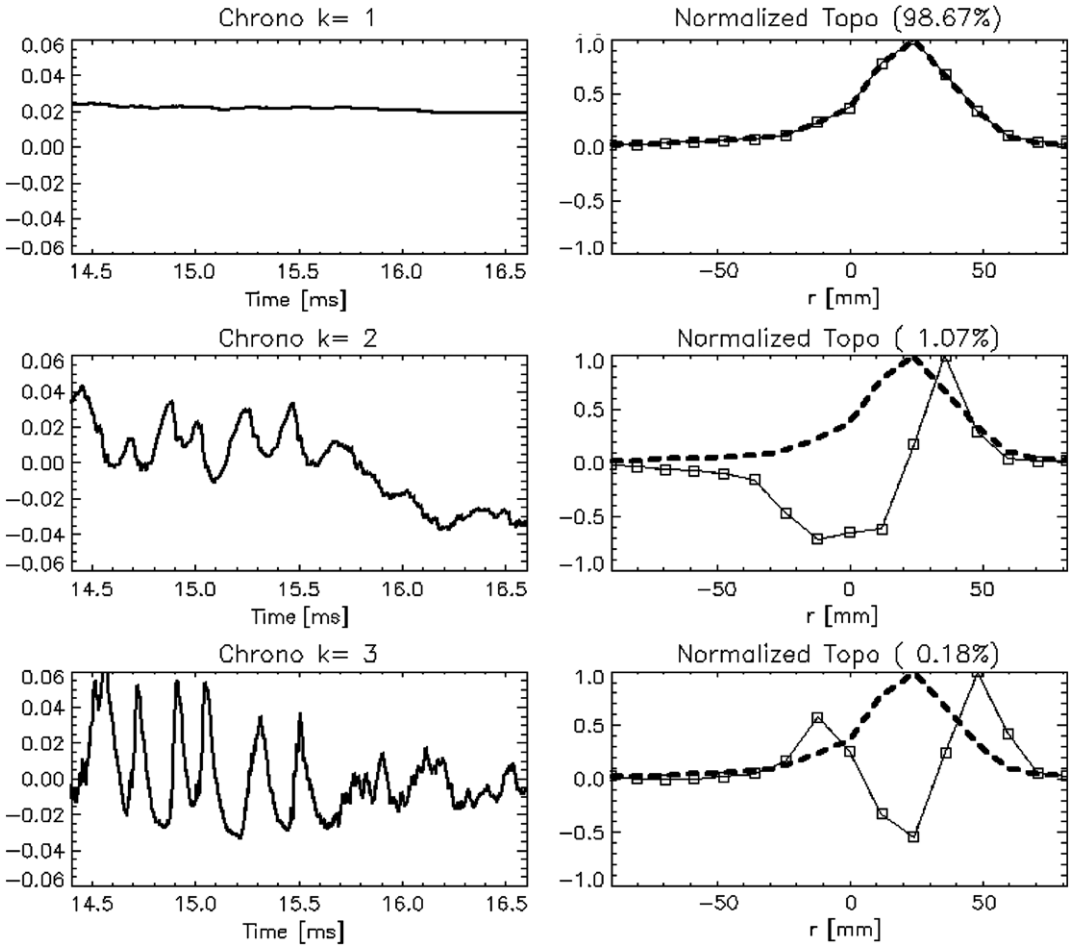

Figure 9. Example of fluctuations analysis of fast bolometric signals from the bottom AXUV array with 1 μs temporal and 1 cm spatial resolution in a shot with edge plasma biasing (#26995, $r_E = 60$ mm, $U_B = +250$ V). Temporal and spatial eigenvectors of the first three significant components of the SVD are drawn and compared with an averaged emission profile (dashed line). Chronos (on the left) show the temporal behaviour of the radiation losses which can be divided into a dominating quasi-stationary spatial part ($k = 1$), a rotating asymmetric component ($k = 2$) and radial structures ($k = 3$). The normalized energy (weight) of each component is given in brackets. Open squares on topos represent chord radii of the individual bolometric channels

3.5. Radiation fluctuation and profile measurements with fast bolometry

Two arrays of fast AXUV-based bolometers (A = advanced) with 16 and 19 channels were installed in the same poloidal cross-section in mutually perpendicular directions (from the LFS and bottom side) to monitor the radiated power profile. This arrangement with unique temporal resolution of 1 μs and spatial resolution of about 1 cm and a very high signal to noise ratio allowed a visualization of fine structures on the radiated power profile. First, the measured AXUV data are typically used to find the evolution of the total radiation, radiation peak position (shift), radiation FWHM and the brightness profile [7]. Later, the data are separated into spatio-temporal components by the singular value decomposition (SVD) method [8]. In this way, components with a different spatial or temporal behaviour can be distinguished from each other and they were here interpreted as the dominating main plasma profile ($k = 1$), a poloidally rotating asymmetric component ($k = 2$) and radial structures corresponding to a symmetric component ($k = 3$), see figure 9. A high contrast between the $k = 1$ component and higher ones, usually of the order of the weight ratios 99.6 : 0.3 : 0.05, is observed for a typical ohmically heated CASTOR plasma. With biasing, higher components are amplified up to 98.5 : 1.1 : 0.2, as shown at the end of the biasing phase in figure 9. Topos, spatial eigenvectors, show the type of evolution (amplitude change, poloidal or radial movement) and a localization of each structure, while chronos, temporal parts, indicate their presence, amplitude and periodicity. In figure 9, a vanishing of the 6 kHz radial and poloidal structures is observed after the end of the biasing phase. The method, based on SVD applied to fast bolometric data was developed during the present HostLab experiment and was later used for the analysis of snake-like structures after pellet injection in the T-10 tokamak [9].

Another method to process fast bolometric data is the analysis of the fluctuating part of raw data obtained by subtracting the mean value. The data are chord integrated, and thus the result does not correspond to the evolution of single local turbulent events but to their sum along the whole chord. By the autocorrelation analysis, the event frequency can be obtained from the periodicity of the autocorrelation function. The cross-correlation of one channel with neighbouring ones in principle gives the velocity and the direction of the movement,

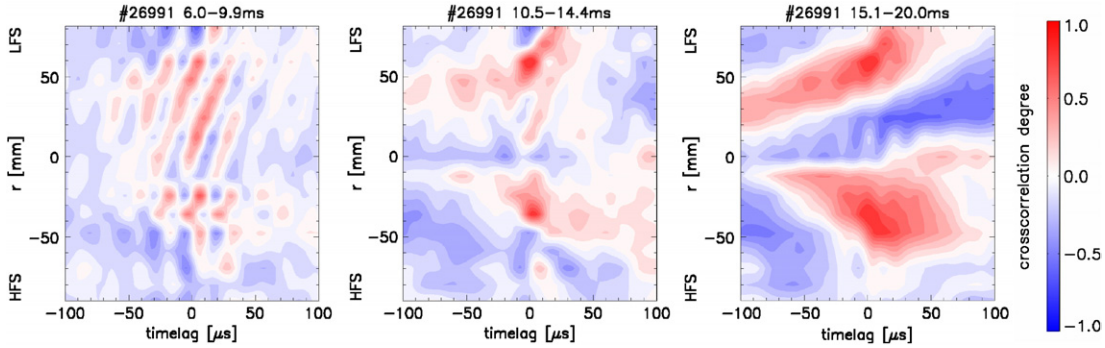

Figure 10. Cross-correlation between one horizontal chord at 40 mm against all bottom chords shows moving structures in shot #26991. Prior to biasing (left figure), the presence of the periodic events with frequency 30 kHz and velocity 2.3 km s^{-1} are demonstrated. During biasing with biasing voltage +150 V (middle figure), the surface near radius 50 mm shows a high level of correlation indicating the presence of well-localized structure. After biasing (right figure), a well-correlated, radially moving event is registered.

while the cross-correlation with a perpendicular bolometric chord gives the localization of the event. As an illustration, the cross-correlation analysis (horizontal chord at 40 mm against bottom chords) of shot #26991 with a biasing period at 10–15 ms is shown in figure 10. Prior to biasing, clear structures with repetition frequency of about 30 kHz are present. During biasing, the periodicity is destroyed, but the surface near radius 50 mm shows a high level of correlation, indicating the presence of a well-localized structure. A few milliseconds after the end of biasing, the periodicity is still not restored; however, a well-correlated, radially moving event is registered.

3.6. Development of standard interfaces for remote participation and data exchange

During the CASTOR experiments, substantial progress has been achieved in the development of tools to bring the scientists involved in the CRP project in close communication. The CRP web page was complemented with dedicated designed interfaces based on the CRP-DASSQL database which allow upload/download of files, discussion forums and will integrate a standard interface for remote participation allowing for remote operation, real time video link and database access of any device (the work is in progress). The web tools under development are being assessed in view of future application to other operating devices.

4. Discussion and conclusions

This 1st Joint (Host Laboratory) Experiment on 'JRUST' has clearly demonstrated that small tokamaks are suitable and important for broad international cooperation, providing the necessary environment and manpower to conduct dedicated joint research programmes. The contribution of small tokamaks to the mainstream fusion research such as edge turbulence, improved confinement and diagnostics development in the present case can be enhanced through coordinated planning [10]. The activities under this IAEA CRP are already paying visible dividends.

The edge plasma and the radial structure of electrostatic edge turbulence were precisely characterized using a double radial array of Langmuir probes. A poloidal array of 96 Langmuir probes was employed to characterize the poloidal structure of edge turbulence, revealing wave-like extended structures. Integrated Hall sensors were tested for the first time in a tokamak environment and found to be an attractive alternative for pick-up coils which require an integration drift removal. Two arrays of fast bolometers provided a visualization of fine structures on the radiated power profile.

The development of remote participation tools is of great interest, and additional collaboration with other tokamaks will help to develop further a standard platform to exchange data from several tokamaks and to allow for remote operation of diagnostics. The goal is to connect the small tokamaks through a network where it would be possible to plan, implement and run experiments to address particular topics taking advantage of the potential of running similar or complementary experiments simultaneously on several machines.

The JE outputs have triggered much interest from the participants to develop further and refine the collaborative research in some of the topics. The second JE took place from 25 September to 6 October 2006 on the tokamak T-10 of the RRC 'Kurchatov Institute' in Moscow. The third JE will take place from 25 to 31 October 2007 on the tokamak ISTTOK of CFN, IST Lisbon.

Acknowledgments

This research has been partially supported by the Grant Agency of the Academy of Sciences of the Czech Republic (grant KJB100430504). Attendance was partially supported through the IAEA and through ICTP grants.

References

[1] Devynck P. *et al* 2005 Spatially resolved characterization of electrostatic fluctuations in the scrape-off layer of the CASTOR tokamak *Plasma Phys. Control. Fusion* **47** 269–80

[2] Stockel J. *et al* 2005 Formation of convective cells during scrape-off layer biasing in the CASTOR tokamak *Plasma Phys. Control. Fusion* **47** 635–43

[3] Van Oost G. *et al* 2003 Turbulent transport reduction by $E \times B$ velocity shear during edge plasma biasing: recent experimental results *Plasma Phys. Control. Fusion* **45** 621–43

[4] Duran I., Stockel J., Mank G., Finken K.H., Fuchs G. and Van Oost G. 2002 First results of magnetic turbulence measurements using an array of Hall detectors in the TEXTOR tokamak *Rev. Sci. Instrum.* **73** 3482

[5] Peleman P. *et al* 2006 Highly resolved measurements of periodic radial relaxation in edge biasing experiments *Int. Conf. on Plasma Surface Interactions (PSI) (Hefei Anhui, China)* 2007 *J. Nucl. Mater.* at press

[6] Gunn J., Stockel J., Adamek J., Duran I., Horacek J., Hron M., Jakubka K., Kryska L., Zacek F. and Van Oost G. 2001 Direct measurements of $E \times B$ flow and its impact on edge turbulence in the CASTOR tokamak using an optimized Gundestrup probe *Czech. J. Phys.* **51** 1001–10

[7] Dufkova E. *et al* 2005 *32nd EPS Conf. on Plasma Physics (Tarragona, 27 June–1 July 2005)* vol 29C (ECA) P-2.074

[8] Dudok T. *et al* 1994 The biorthogonal decomposition as a tool for investigating fluctuations in plasmas *Phys. Plasmas* **1** 3288–300

[9] Weinzettl V. *et al* 2006 *33nd EPS Conf. on Plasma Physics (Roma, 19–23 June 2006)* (ECA) P-4.080

[10] Gryaznevich *et al* M.P. 2005 Joint research using small tokamaks *Nucl. Fusion* **45** S245–54